Structural analysis of Stc1 provides insights into the coupling of RNAi and chromatin modification

Chao He[a], Sreerekha S. Pillai[b,c,1], Francesca Taglini[b,c,1], Fudong Li[a], Ke Ruan[a], Jiahai Zhang[a], Jihui Wu[a], Yunyu Shi[a,2], and Elizabeth H. Bayne[b,c,2]

[a]Hefei National Laboratory for Physical Sciences at Microscale and School of Life Sciences, University of Science and Technology of China, Hefei, Anhui 230026, China; [b]Wellcome Trust Centre for Gene Regulation and Expression, College of Life Sciences, University of Dundee, Dundee DD1 5EH, United Kingdom; and [c]Institute of Cell Biology, School of Biological Sciences, University of Edinburgh, Edinburgh EH9 3JR, United Kingdom

Edited by Gregory J. Hannon, Cold Spring Harbor Laboratory, Cold Spring Harbor, NY, and approved April 2, 2013 (received for review July 17, 2012)

Noncoding RNAs can modulate gene expression by directing modifications to histones that alter chromatin structure. In fission yeast, siRNAs produced via the RNAi pathway direct modifications associated with heterochromatin formation. siRNAs associate with the RNAi effector protein Argonaute 1 (Ago1), targeting the Ago1-containing RNA-induced transcriptional silencing (RITS) complex to homologous nascent transcripts. This promotes recruitment of the Clr4 complex (CLRC), which mediates methylation of histone H3 on lysine 9 (H3K9me) in cognate chromatin. A key question is how the RNAi and chromatin modification machineries are connected. Stc1 is a small protein recently shown to associate with both Ago1 and CLRC and to play a pivotal role in mediating the RNAi-dependent recruitment of CLRC to chromatin. To understand its mode of action, we have performed a detailed structural and functional analysis of the Stc1 protein. Our analyses reveal that the conserved N-terminal region of Stc1 represents an unusual tandem zinc finger domain, with similarities to common LIM domains but distinguished by a lack of preferred relative orientation of the two zinc fingers. We demonstrate that this tandem zinc finger domain is involved in binding Ago1, whereas the nonconserved C-terminal region mediates association with CLRC. These findings elucidate the molecular basis for the coupling of RNAi to chromatin modification in fission yeast.

NMR | *Schizosaccharomyces pombe*

RNAi is a conserved gene silencing mechanism characterized by the involvement of small RNAs. These small RNAs are bound by Argonaute proteins, forming RNAi effector complexes that can mediate silencing of specific targets based on sequence homology (1). This silencing can occur either posttranscriptionally, via transcript cleavage or translational repression, or at the transcriptional level, via chromatin modification. Such RNAi-dependent chromatin modification has been implicated in genome regulation throughout eukaryotes; however, mechanisms underlying the coupling of RNAi to either DNA methylation and/or histone modification remain poorly understood in most systems (2, 3).

One of the best-characterized examples of RNAi-directed chromatin modification occurs in the fission yeast, *Schizosaccharomyces pombe*, where RNAi is required to promote assembly of pericentromeric heterochromatin. Heterochromatin is a specialized form of chromatin that is generally associated with transcriptional repression, and it is important for genome stability. In fission yeast, as in higher eukaryotes, heterochromatin is characterized by high levels of methylation on lysine 9 of histone H3 (H3K9), which provides a binding site for chromodomain proteins, including the heterochromatin protein 1 (HP1) family proteins Swi6 and Chp2 (4–6). Assembly of heterochromatin in fission yeast requires the action of histone deacetylases (Sir2, Clr3, and Clr6) as well as the sole H3K9 methyltransferase, Clr4 (7–9). Clr4 resides in a multisubunit Clr4 complex (CLRC), all members of which are required to support Clr4-mediated H3K9 methylation. These include the cullin protein Cul4, the β-propeller protein Rik1, the WD-40 protein Dos1 (Raf1), and Dos2 (Raf2) (10–14). Cul4 serves as a scaffold for E3 ubiquitin ligase complexes, and Rik1 and Dos1 can be structurally aligned with the human E3 ligase complex components DDB1 and DDB2, respectively (15). However, although CLRC exhibits ubiquitin ligase activity in vitro, whether CLRC acts as an ubiquitin ligase in vivo is not known (11).

Both RNAi and DNA binding proteins contribute to the recruitment of CLRC to chromatin, with their relative importance varying between heterochromatic loci (16–19). At the repetitive sequences flanking centromeres, RNAi is important for both establishment and maintenance of Clr4-mediated H3K9 methylation (6, 20). Transcription of the pericentromeric repeats during S phase gives rise to dsRNA that is processed by Dicer into siRNAs (21–25). These siRNAs are loaded into the Argonaute protein Ago1, targeting the Ago1-containing RNA-induced transcriptional silencing (RITS) complex to homologous nascent transcripts. RITS recruits further factors, including the RNA-dependent RNA polymerase complex (RDRC), which promote the generation of further centromeric siRNAs, thereby amplifying the RNAi response (26–28). Ago1 is associated in RITS with the GW protein Tas3, and the chromodomain protein Chp1. Chp1 can bind methylated H3K9, thereby stabilizing and propagating RITS association with heterochromatic domains (29, 30). Recruitment of RITS to chromatin is thus reinforced by both RNAi-dependent and RNAi-independent positive feedback loops. Ultimately, chromatin-bound RITS promotes recruitment of CLRC, resulting in targeted H3K9 methylation that can subsequently spread to form large heterochromatin domains (5, 31).

A key question in all siRNA-directed chromatin modification systems is how RNAi and chromatin modification are connected. In fission yeast, recent evidence suggests that the pivotal interaction between RITS and CLRC is mediated by Stc1 (31). Initially identified in a genetic screen for factors required for pericentromeric heterochromatin integrity, Stc1 was shown to be required specifically for RNAi-dependent H3K9 methylation and to associate with both RITS (Ago1) and CLRC components in vivo. Moreover, artificial tethering of Stc1 to a euchromatic

Author contributions: C.H., Y.S., and E.H.B. designed research; C.H., S.S.P., F.T., J.Z., and J.W. performed research; C.H., S.S.P., F.T., F.L., K.R., Y.S., and E.H.B. analyzed data; and C.H., Y.S., and E.H.B. wrote the paper.

The authors declare no conflict of interest.

This article is a PNAS Direct Submission.

Data deposition: The atomic coordinates for the ensemble of structures representing the solution structure of the Stc1 tandem zinc finger domain have been deposited in the Protein Data Bank, www.pdb.org (PDB ID code 2LUY); and the chemical shift assignment data have been deposited in the BioMagResBank, www.bmrb.wisc.edu (accession no. 18546).

[1]S.S.P. and F.T. contributed equally to this work.

[2]To whom correspondence may be addressed. E-mail: yyshi@ustc.edu.cn or elizabeth.bayne@ed.ac.uk.

See Author Summary on page 8331 (volume 110, number 21).

This article contains supporting information online at www.pnas.org/lookup/suppl/doi:10.1073/pnas.1212155110/-/DCSupplemental.

locus was sufficient to trigger silencing and heterochromatin assembly independent of RNAi. Together, these findings indicate that Stc1 functions at the interface between RNAi and chromatin modification, likely mediating the recruitment of CLRC to target chromatin via interaction with nascent transcript-bound RITS.

Despite the pivotal role of Stc1 in the RNAi-directed chromatin modification pathway, relatively little is known about its molecular function. Bioinformatic analyses have indicated that the N-terminal region of Stc1 bears similarity to LIM-type tandem zinc finger domains, and mutations in the putative second zinc finger have been found to disrupt the association of Stc1 with Ago1 (31). Interestingly, LIM domain proteins were also recently shown to associate with Argonaute proteins in mammalian cells, facilitating microRNA (miRNA)-directed translational repression (32). However, little is known about the structural basis of the interactions in either case. To investigate the nature of the Stc1 protein and its mode of action, we analyzed the structure of the protein by NMR. Our data reveal that the N terminus of Stc1 does form a tandem zinc finger domain, but with an organization distinct from that of other zinc finger motifs, including LIM domains; in particular, the two zinc finger modules show little preferred orientation with respect to one another. Nevertheless, in vivo and in vitro analyses indicate that both zinc fingers contribute to the binding of Ago1, defining this tandem zinc finger domain as an Argonaute-interaction motif. In addition, we demonstrate that association with CLRC is mediated by the unstructured C-terminal region of Stc1. Our findings elucidate the molecular basis for the Stc1-mediated coupling of chromatin modification to RNAi.

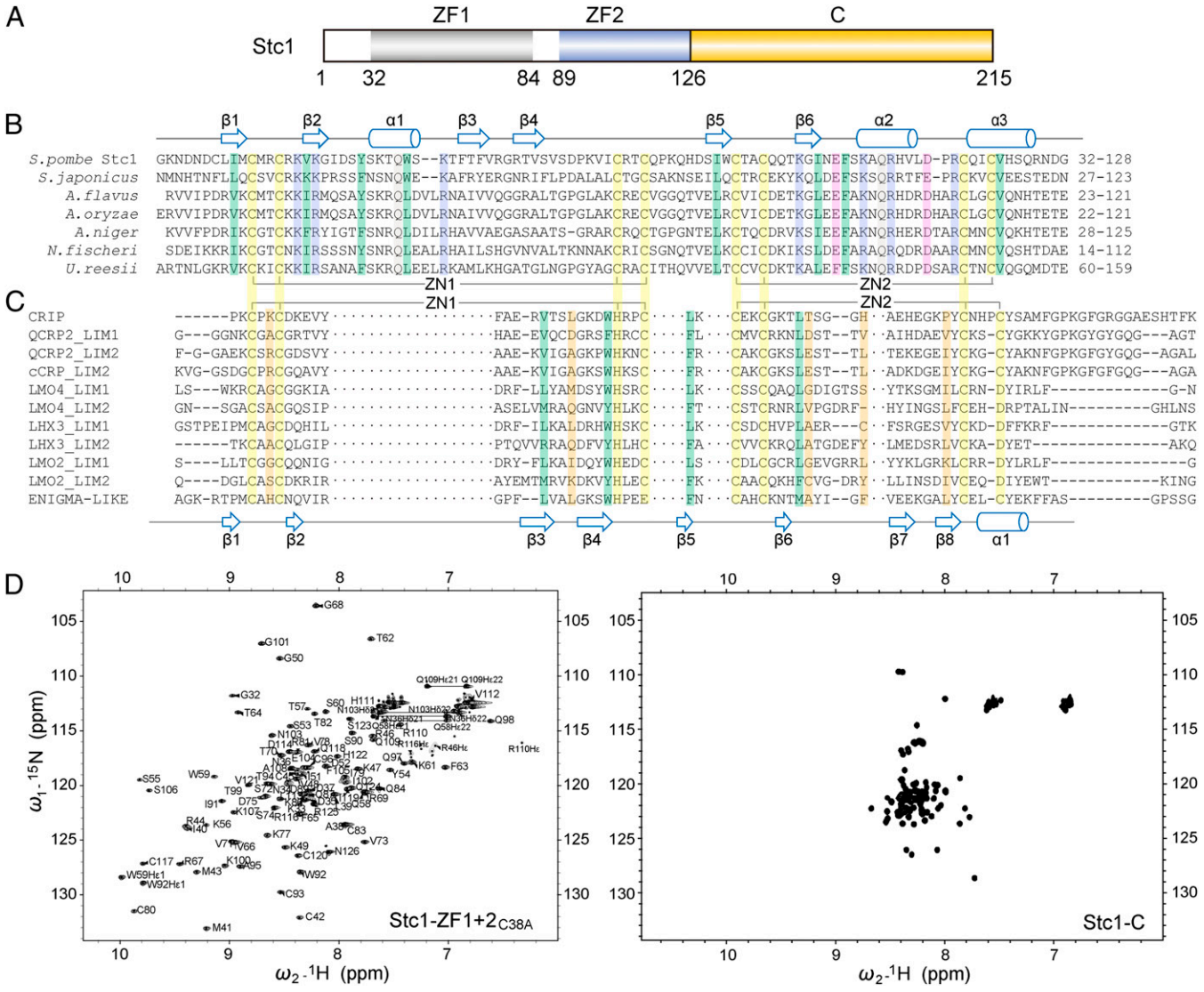

Fig. 1. Domain architecture of fission yeast Stc1. (*A*) Domain organization of fission yeast Stc1, illustrating the positions of the two zinc fingers (ZF1 and ZF2) and C-terminal domain (C). (*B* and *C*) Structure-based sequence alignments of the N-terminal conserved region of Stc1 with homologous proteins and common LIM domains. Sequences in *B* were obtained from a National Center for Biotechnology Information protein BLAST search and are named according to species abbreviation. Accession numbers and full species names are as follows: gi|19113327| (Stc1) *S. pombe*, gi|213405689| *Schizosaccharomyces japonicus*, gi|238496859| *Aspergillus flavus*, gi|317146914| *Aspergillus oryzae*, gi|317027448| *Aspergillus niger*, gi|119481491| *Neosartorya fischeri*, and gi|258565501| *Uncinocarpus reesii*. Conserved residues are colored as follows: yellow (zinc-coordinating), green (hydrophobic or aromatic), gray (polar uncharged), blue (positively charged), and pink (negatively charged). In *C*, the substitutable residues, responsible for differences in relative orientation of the two zinc binding modules, are highlighted in orange. Stc1 secondary structures are shown above *B*, and LIM domain secondary structures are shown below *C*. (*D*) Assigned ^{1}H-^{15}N HSQC spectra of Stc1-ZF1+2$_{C38A}$ (*Left*) and Stc1-C (*Right*) acquired at 25 °C.

Results

Domain Architecture of Stc1. Sequence alignments reveal a conserved region in the N terminus of Stc1 containing eight invariant cysteine residues (31) (Fig. 1 *A* and *B*). To investigate the domain architecture of Stc1, we expressed and purified recombinant proteins corresponding to the conserved N-terminal region [residues 32–126, incorporating the tandem zinc finger (ZF), and referred to as Stc1-ZF1+2] and the C-terminal region (residues 127–215, referred to as Stc1-C) for structural study. The eight conserved cysteines in Stc1-ZF1+2 are predicted to coordinate two zinc ions per molecule, which was supported by atomic absorption spectroscopy (500 μL of 0.5 mM protein sample has 35.47 μg of zinc). An additional nonconserved cysteine (Cys^{38}) was mutated to alanine to avoid molecular dimerization caused by cysteine oxidation; ^{1}H NMR spectra for the mutant (Stc1-ZF1+2_{C38A}) and native (Stc1-ZF1+2) proteins are almost identical (Fig. S1), indicating that this mutation does not have an impact on the overall folding of the protein. In 2D NMR analyses, the ^{1}H-^{15}N heteronuclear single-quantum coherence (HSQC) spectrum of Stc1-ZF1+2_{C38A} is well dispersed, indicating a well-defined global folding of this structural domain (Fig. 1*D*). In contrast, the poorly dispersed spectrum of Stc1-C suggests that this region is largely unstructured. A dynamically disordered state of Stc1-C was further confirmed by CD spectroscopy (Fig. S2). We therefore conclude that Stc1 has a conserved zinc finger domain in its N terminus and a nonconserved, unstructured C-terminal region.

Solution Structure of the Stc1 Tandem Zinc Finger Domain. We determined the solution structure of Stc1-ZF1+2_{C38A} by multidimensional heteronuclear NMR spectroscopy (Fig. 2 and Table 1). This revealed that Stc1-ZF1+2_{C38A} forms two C4 zinc fingers, comprising amino acids 32–84 (ZF1) and 89–126 (ZF2) (Fig. 1*A*). The two zinc fingers of Stc1 are each well defined by the NMR data, with rmsd values for the heavy atoms of the 20 lowest energy structures of ZF1 and ZF2 both calculated close to 1.0 Å (Table 1).

Each zinc finger domain employs an orthogonal arrangement (Fig. 2*A*). ZF1 begins with a well-defined antiparallel β-sheet (sheet 1, β1–β2, residues Leu^{39}-Met^{41} and Val^{48}-Gly^{50}) connected via a rubredoxin-type turn (33) that accommodates the zinc coordinating residues Cys^{42} and Cys^{45}. It is followed by a short α-helix (α1, residues Lys^{56}-Ser^{60}) that is oriented perpendicular to sheet 1 and then by a second antiparallel β-sheet (sheet 2, β3-β4, residues Phe^{63}-Val^{66} and Arg^{69}-Ser^{72}) that extends outwards. This second β-sheet appears to have a slightly increased mobility relative to the rest of the domain, because measurement of backbone heteronuclear ^{1}H-^{15}N NOEs, a sensitive indicator of residue internal motions, revealed lower than average values for this region (Fig. S3*C*). Furthermore, the backbone rmsd value for ZF1 was reduced from 0.61 Å to 0.49 Å when this region was excluded (Table 1). Following a loop that resides near helix 1, a turn accommodating the coordinating Cys^{80} and Cys^{83} terminates the first C4 zinc finger domain.

ZF2 displays a tertiary structure similar to ZF1 (Fig. 2*A*). The two strands of a third antiparallel β-sheet (sheet 3, β5-β6, residues Ser^{90}-Trp^{92} and Thr^{99}-Gly^{101}) are connected by a turn that includes zinc-coordinating Cys^{93} and Cys^{96}. Following a loop, which is oriented orthogonal to sheet 3, a second short α-helix (α2, residues Lys^{107}-His^{111}) replaces the flexible sheet 2 of ZF1. A short α-helix (α3, residues Gln^{118}-Ser^{123}) ends the second C4 zinc finger, accommodating the zinc-coordinating Cys^{117} and Cys^{120}.

Dynamic Properties of the Stc1 Tandem Zinc Finger Domain. Although the individual zinc fingers can be well resolved by NMR, the overall structure of the Stc1 tandem zinc finger domain does not converge to one single conformation, likely due to flexibility in the interdomain linker (Fig. 2*B*). The structure of the linker (residues Pro^{85}-His^{88}) is poorly defined by the experimental data because residue His^{88} is invisible in the ^{1}H-^{15}N HSQC spectrum and residues Lys^{86} and Gln^{87} are overlapped in the center of the spectrum. To examine whether this reflects a true conformational flexibility rather than a lack of observed NOEs, we have further investigated the dynamic properties of the Stc1 tandem zinc finger domain using ^{15}N relaxation measurement (Fig. S3). The trimmed mean ratio of NMR R_2-to-R_1 relaxation rates, R_2/R_1 (*Materials and Methods*), which is related to the overall tumbling of the protein, was lower for ZF2 (10.8 ± 1.0) compared with ZF1 (14.5 ± 2.6), consistent with the smaller size of ZF2 if the two domains relax independently (34).

To assess the tandem domain orientation further, we determined the ^{1}H-^{15}N residual dipolar couplings (RDCs) using two alignment media: 3% C12E5/hexanol mixture (C12E5/hexanol, Fig. S4*A*) and 5% stretched polyacrylamide gel (GEL, Fig. S4*B*). The experimental backbone ^{1}H-^{15}N RDCs are in reasonable agreement with the best-fit values for the individual zinc finger domains in both media, indicating that each domain can be refined to a high precision using RDCs (Fig. S4 *C* and *D*). In both media, the derived alignment tensors for the two zinc finger domains were significantly different (Table S1), indicating that the two domains are not coordinately oriented by a common interaction with the media (35). Interestingly, differences in the largest principal axis component of the alignment tensor (Azz) between the two media were greater for ZF1 than for ZF2, which may relate to the higher anisotropy of the shape and electrostatic charge distribution of ZF1, causing it to experience a relatively higher degree of alignment in GEL compared with C12E5/hexanol. Taken together, the observed differences in

Table 1. Structure calculation restraints and structural statistics for the 20 lowest energy structures of the Stc1 tandem zinc finger domain

Distance restraints	1,642
Intraresidue	772
Sequential (|i − j| = 1)	345
Medium-range (2 ≤ |i − j| ≤ 4)	186
Long-range (|i − j| ≥ 5)	335
Hydrogen bonds	4
Dihedral angle restraints	140
Dipolar coupling restraints	55
Zinc coordination restraints	28
rmsd from mean structure:	
Backbone/heavy atoms, Å	
Residues 39–84 (ZF1)	0.610/1.160
Residues 39–62, 73–84 (ZF1 excluding sheet 2, β3–β4)	0.495/1.070
Residues 90–123 (ZF2)	0.401/1.067
rmsd from experimental restraints	
NOE distances, Å	0.029 ± 0.002
Dihedral angles, °	0.342 ± 0.128
Dipolar couplings, Hz	0.144 ± 0.031
rmsd from idealized geometry	
Bonds, Å	0.003 ± 0.000
Angles, °	0.694 ± 0.088
Impropers, °	0.306 ± 0.016
Ramachandran plot, %*	
Residues in most favored regions	85.4
Residues in additional allowed regions	14.3
Residues in generously allowed regions	0.3
Residues in disallowed regions	0.0

None of the structures exhibits distance violations greater than 0.5 Å, dihedral angle violations bigger than 5°, or RDC violations larger than 1.5 Hz. *Calculated using nonglycine and nonproline residues 39–84 and 90–123 with the program PROCHECK-NMR to access the quality of the structure.

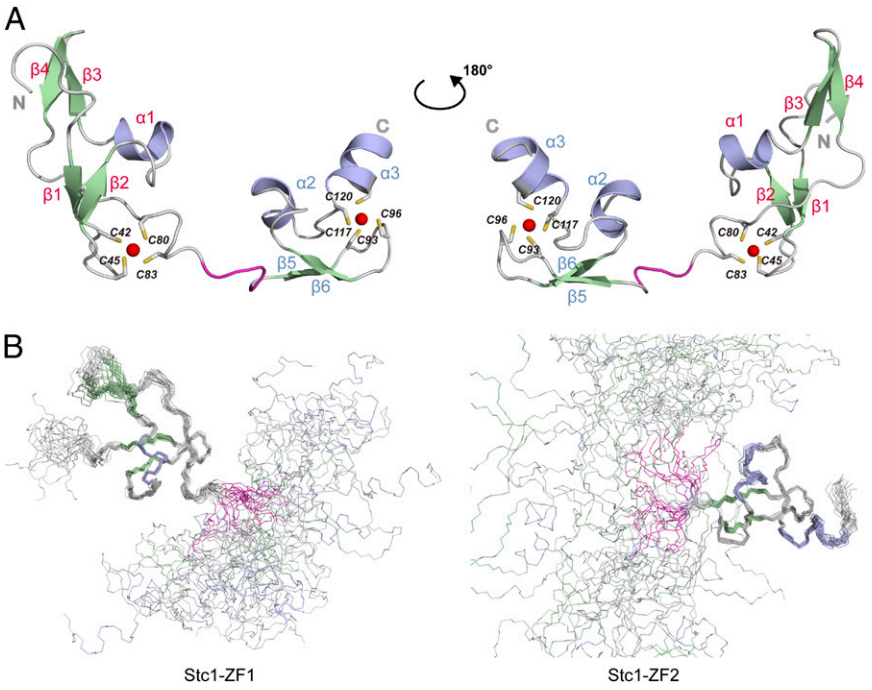

Fig. 2. Three-dimensional structure of the tandem zinc fingers of Stc1. (*A*) Ribbon representations of the NMR lowest energy structure of the Stc1 conserved N-terminal region from different angles. β-Strands are shown in green, and α-helixes are shown in blue. The interdomain linker is shown in magenta, zinc atoms are represented by red spheres, and the zinc-coordinating cysteines are shown as sticks. (*B*) Superimposition of the backbone atoms (N, C_α, and C′) of 20 final NMR structures of Stc1-ZF1 (*Left*) and Stc1-ZF2 (*Right*). Note that the structures cannot be superimposed over the entire molecule, indicating dynamic interdomain motions.

R_2/R_1 ratios and derived alignment tensors indicate that the two zinc fingers are not rigidly positioned as a single fold unit but rather undergo dynamic interdomain motions, and that the interdomain linker is therefore indeed flexible.

The Stc1 Tandem Zinc Finger Is Distinct from Common LIM Domains. To investigate the similarity of the Stc1 tandem zinc fingers to other known structures in the Protein Data Bank (PDB) database, we performed structure-based homology searches using Dali (36). No meaningful similarity was found for ZF1. For ZF2, we found 40 hits, all of them PHD domains, including PHD finger protein 8 (PHF8; PDB ID code 3kv4_A), which had the highest Z-score of 2.7. However, although comparison of the structures of ZF2 and the corresponding region of PHF8 does indicate modest similarity (Fig. S5), the low sequence homology and lack of conserved residues mean this similarity is likely restricted to the protein fold level.

The conserved N-terminal region of Stc1 has previously been predicted to have statistically significant similarity to LIM domains (31) (Fig. 1*C*). We therefore compared the structure of the Stc1 tandem zinc finger domain with those of common LIM domains. Some common properties can be observed: Both adopt tandem zinc-finger topologies (Fig. 3*A*), and both exhibit similar structural features around the zinc binding sites, with treble-clef folds (37, 38) coordinating the zinc ions (Fig. S6). Moreover, both zinc fingers of Stc1 use orthogonal folding patterns similar to those of LIM domains (Fig. 3*A*). However, the secondary structure arrangement of the Stc1 tandem zinc finger domain is appreciably different from common LIM domains. Stc1-ZF1 contains an extra α-helix between the first and second antiparallel β-sheets, and the second β-sheet extends outward and is relatively flexible. In addition, Stc1-ZF2 contains a second α-helix in place of the fourth antiparallel β-sheet of the LIM domain. Most significantly, in LIM domains, the tandem zinc fingers are arranged in a preferred orientation relative to one another, forming a single fold unit, whereas Stc1 tandem zinc fingers fold separately, allowing them to undergo dynamic interdomain motions (Fig. 3 *B* and *C*).

The relatively rigid packing of LIM-type tandem zinc fingers appears to relate to the short linker length (two residues), as well as to the positioning of several conserved hydrophobic or aromatic residues at the interface between the two modules that contribute to the overall fold (Figs. 1*C* and 3*B*, residues highlighted in green). The relative orientations of LIM domain zinc fingers can nevertheless vary to some extent, for instance, due to additional interdomain contacts involving less well-conserved residues (Figs. 1*C* and 3*B*, residues highlighted in orange). In contrast, however, in Stc1, the zinc finger modules are separated by a longer, largely nonconserved linker, and many of the conserved hydrophobic/aromatic or polar uncharged residues important for protein folding protrude into the inner cores of their respective zinc fingers, rather than outward between domains (e.g., Tyr^{54}, Trp^{59}, and Phe^{105} in Figs. 1*C* and 3*B*). These differences could explain why, in contrast to LIM domains, the Stc1 tandem zinc fingers fold independently and with little preferred orientation with respect to one another.

The Tandem Zinc Finger Domain of Stc1 Is Required for Interaction with Ago1 but Not CLRC. Point mutations affecting two conserved residues in the Stc1 tandem zinc finger domain (Lys^{100} or Arg^{116}) were previously found to disrupt the association of Stc1 with Ago1 (31). Both of these residues can be mapped to the electrostatic potential surface of ZF2, implicating at least ZF2 in Ago1 binding (Figs. 1*B* and 3*D*). To further investigate the function of the entire tandem zinc finger domain of Stc1, we generated yeast strains in which the endogenous *stc1*$^+$ gene was replaced in the genome by versions lacking either one or both zinc fingers (ΔZF1, ΔZF2, and ΔZF1+2; Fig. 4*A*). All three mutant proteins were found to be stably expressed in vivo (Fig. S7*A*). The ability of the truncated Stc1 proteins to function in RNAi-dependent heterochromatin assembly was assessed via silencing of a pericentromeric *ade6*$^+$ marker gene. In WT cells, the presence of

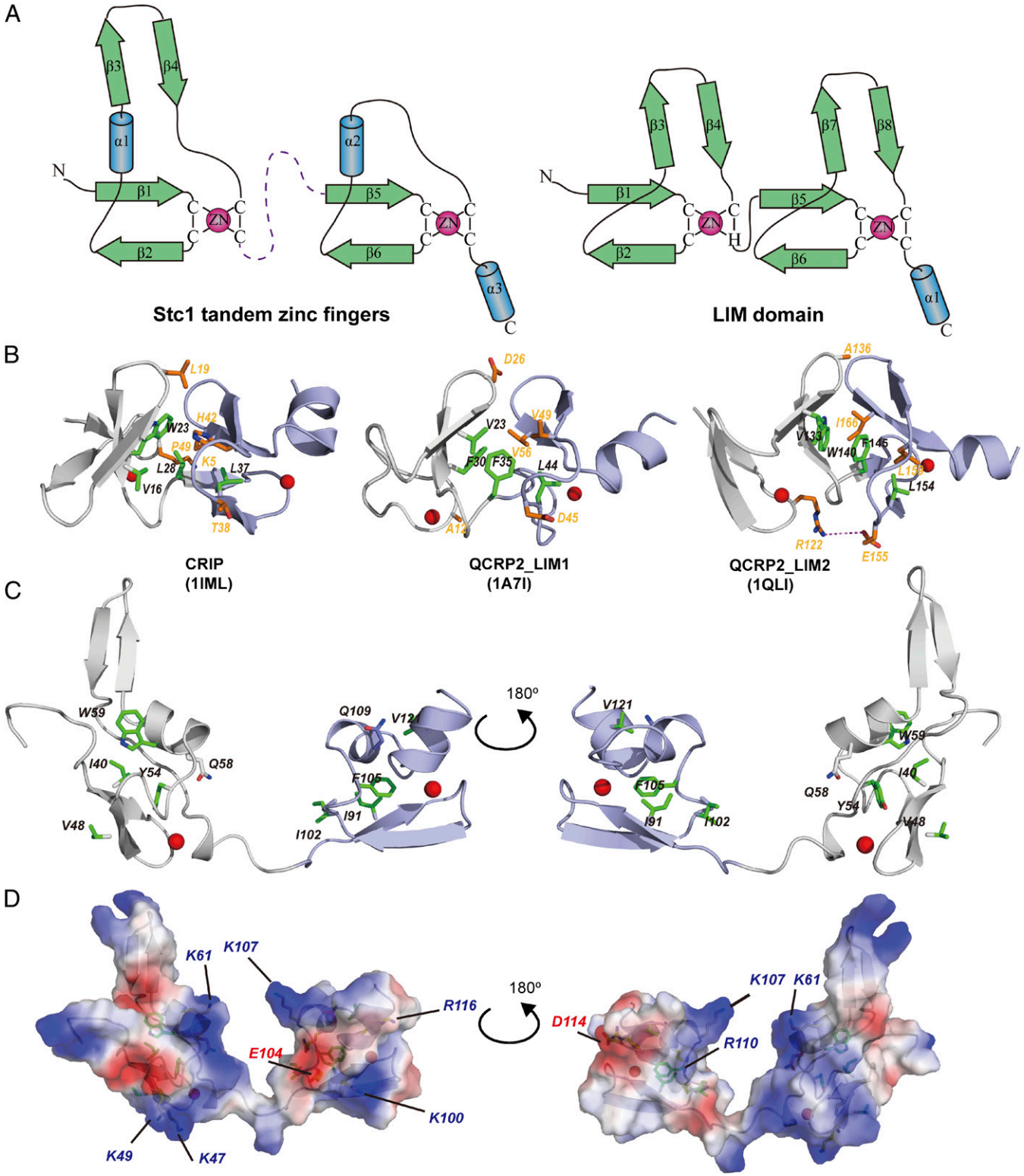

Fig. 3. Comparison of the Stc1 tandem zinc finger domain with known LIM domains. (*A*) Topology of the Stc1 tandem zinc finger domain and a LIM domain. Green arrows represent β-strands, and blue cylinders represent short α-helices. The poorly defined interdomain linker of Stc1 is represented by the dotted line. (*B*) Ribbon representations of LIM domains CRIP, QCRP2_LIM1, and QCRP2_LIM2 (PDB ID codes in parenthesis). (*C*) Ribbon representations of the Stc1 tandem zinc finger domain. N- and C-terminal zinc binding modules are depicted in gray and blue, respectively; zinc atoms are represented by red spheres. Conserved hydrophobic and aromatic residues, determining overall domain folding, are shown in green. Substitutable residues responsible for differences in relative orientation of the two zinc fingers are shown in orange. (*D*) Electrostatic potential surfaces of the Stc1 tandem zinc fingers, shown in the same orientations as in *C*. Conserved positively and negatively charged residues are highlighted in blue and red, respectively.

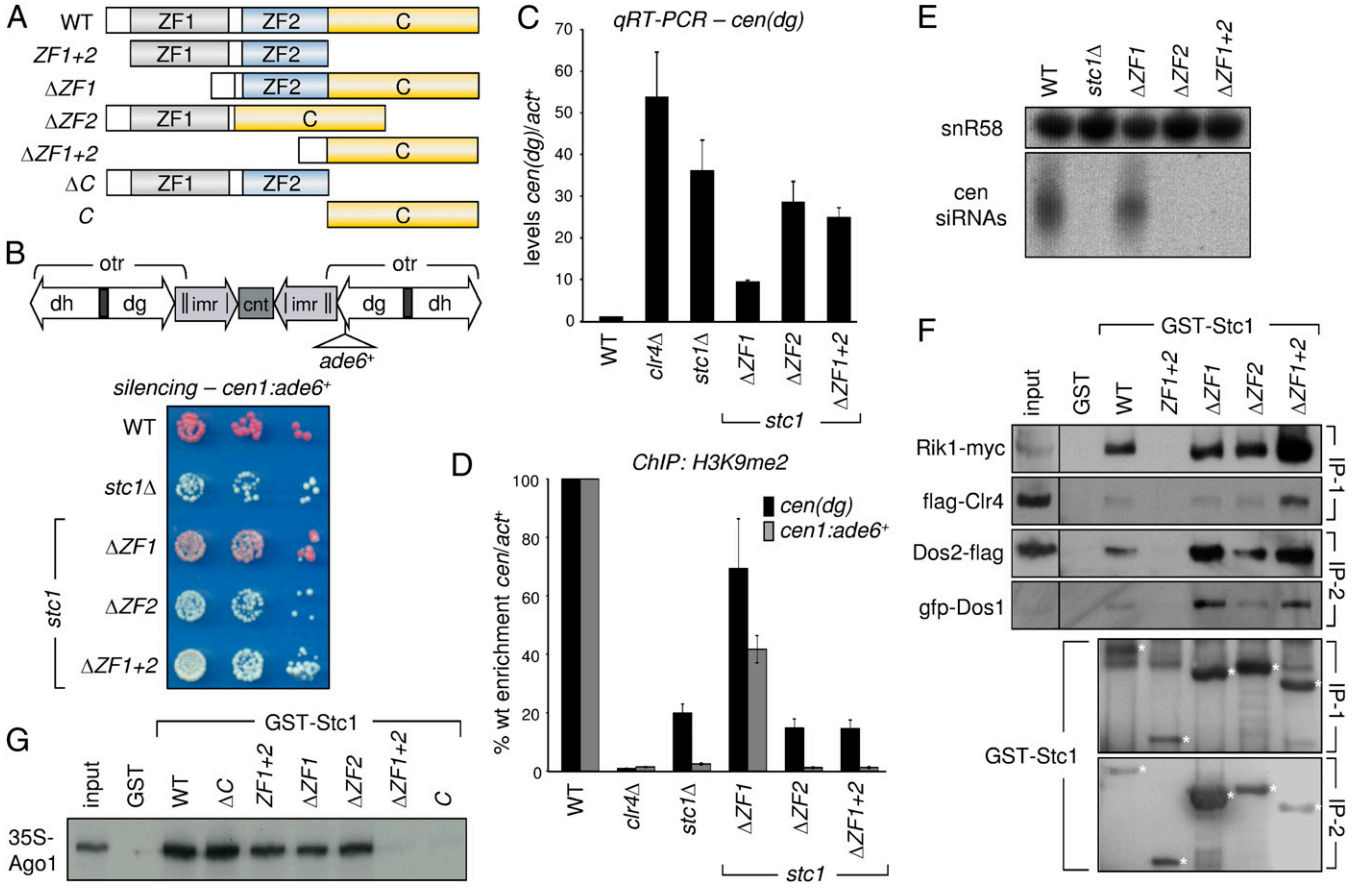

Fig. 4. Stc1 tandem zinc finger domain is required for interaction with Ago1 but not CLRC. (*A*) Schematic of Stc1 domain deletion mutants analyzed. (*B*) Assay for silencing at *cen1:ade6*$^+$. The schematic shows the position of the *cen1:ade6*$^+$ marker gene in centromere 1 (cen1), relative to outer repeat (*otr*) *dg* and *dh* elements, innermost repeats (*imr*), and central core (*cnt*). Cells are plated on media containing limiting adenine, where silencing of *cen1:ade6*$^+$ results in red colonies and loss of silencing results in pink/white colonies. (*C*) Quantitative RT-PCR analysis of *cen(dg)* transcript levels relative to *act1*$^+$, normalized to WT ($n = 3$). (*D*) ChIP analysis of H3K9me2 levels associated with *cen(dg)* and *cen1:ade6*$^+$, relative to *act1*$^+$, normalized to WT ($n = 3$). (*E*) Northern blot analysis of centromeric siRNAs (snoRNA58 is a loading control). (*F*) GST-Stc1 pull-downs from cell lysates. Recombinant GST-tagged WT or mutant Stc1 proteins were incubated with equal fractions of the same cell lysate prepared from *S. pombe* strains expressing Rik1-myc and flag-Clr4 [immunoprecipitation (IP)-1] or Dos2-flag and gfp-Dos1 (IP-2). Precipitated proteins were analyzed by Western blot; the input corresponds to 0.5% of the lysate volume used for each IP. GST-Stc1 proteins are indicated by asterisks (note that Stc1 exhibits a shift in apparent molecular weight that is lost on deletion of the C-terminal domain). (*G*) In vitro binding assay with recombinant GST-tagged WT or mutant Stc1 proteins and ^{35}S-labeled Ago1.

heterochromatin silences the *ade6*$^+$ gene, resulting in red colonies on media containing limiting adenine. When heterochromatin is disrupted, for example, on deletion of *stc1*$^+$, *ade6*$^+$ is expressed and the colonies turn white (Fig. 4*B*). Consistent with previous observations for the ZF2 point mutants (31), deletion of ZF2, or ZF1+2, resulted in loss of pericentromeric silencing (Fig. 4*B*). These mutants display increased accumulation of pericentromeric transcripts, reduced levels of H3K9 dimethylation (H3K9me2), and no detectable siRNAs, similar to a *stc1*Δ null mutant (Fig. 4 *C–E*). Surprisingly, however, deletion of ZF1 caused only partial alleviation of silencing, as indicated by variegating pink/white colonies, intermediate levels of pericentromeric transcripts, and a modest reduction in H3K9me2 levels. Deletion of ZF1 also had little effect on centromeric siRNA accumulation (Fig. 4 *B–E*). These observations imply that ZF1 is not absolutely required for Stc1 function, and therefore is not essential to mediate association with either Ago1 or CLRC, although it may contribute to binding by one or more neighboring domains.

We went on to perform pull-down assays to investigate the role of the tandem zinc finger domain in specific protein–protein interactions. We expressed and purified recombinant GST fusion proteins corresponding to WT Stc1, Stc1 lacking one or both zinc finger domains, and the Stc1 tandem zinc finger domain alone (Fig. 4*A* and Fig. S7*B*). To assess interactions with the CLRC complex, we carried out GST pull-down assays using cell lysates from yeast strains expressing epitope-tagged CLRC components. Clr4, Rik1, Dos1, and Dos2 all coprecipitated with full-length Stc1 (Fig. 4*F*), consistent with Stc1 association with the intact CLRC complex (31). On the other hand, truncated Stc1 protein comprising only the tandem zinc finger domain (ZF1+2) did not pull down CLRC components. Strikingly, however, Stc1 proteins lacking one or both zinc fingers (ΔZF1, ΔZF2, and ΔZF1+2) were still able to pull down all tested CLRC components, similar to WT Stc1. This indicates that the tandem zinc finger domain of Stc1 is dispensable for interaction with CLRC.

We used an in vitro binding assay to assess the ability of the Stc1 mutant proteins to interact with Ago1. This approach was used previously to demonstrate a direct interaction between Stc1 and Ago1, and it circumvents the problem that, in vivo, association of Ago1 with Stc1 is lost when any part of the pathway is disrupted (31). Consistent with previous observations, we observed a specific interaction between full-length GST-Stc1 and ^{35}S-labeled Ago1 (Fig. 4*G*). Ago1 binding was unaffected by deletion of the Stc1 C-terminal domain; indeed, the tandem zinc-finger domain alone exhibited Ago1 binding similar to that of full-length Stc1. Interestingly, individual deletions of either ZF1

or ZF2 also had little effect on Ago1 binding, whereas binding was lost on deletion of both zinc fingers (Fig. 4*G*). These observations indicate that, in vitro, association of Stc1 with Ago1 depends on the tandem zinc finger domain and involves both zinc fingers. The partial defect in silencing observed on deletion of ZF1 in vivo (Fig. 4 *B–E*) is therefore most likely explained by a contributory role for this motif in Ago1 binding, in concert with ZF2. Thus, together, these data indicate that interaction with Ago1, but not CLRC, depends on the tandem zinc finger domain of Stc1.

Stc1 C-Terminal Domain Is Required for Binding CLRC. The GST pull-down experiments described above indicate that association with CLRC requires the Stc1 C terminus but not the tandem zinc finger domain. To confirm whether the zinc finger domain is indeed dispensable for Stc1 function in recruitment of CLRC to chromatin, we used an artificial tethering assay that uncouples the functions of Stc1 in Ago1 binding and CLRC recruitment. In this system, a Tet repressor (TetR) DNA binding domain is fused to Stc1 (TetR-Stc1), promoting its recruitment to tet operator (*tetO*) DNA binding sites inserted adjacent to an *ade6*$^+$ reporter gene (*TetO-ade6*$^+$). This artificial recruitment of Stc1 is sufficient to trigger silencing and heterochromatin assembly at an otherwise euchromatic locus (31). Importantly, this silencing is dependent on CLRC but independent of RNAi, because the requirement for RNAi-mediated targeting of Stc1 to chromatin (via interaction with Ago1) is bypassed. As shown previously, in the absence of tethered Stc1, the *TetO-ade6*$^+$ reporter gene is expressed, resulting in white colonies, whereas tethering of WT Stc1 results in a high frequency of red colonies, indicating silencing of the *ade6*$^+$ reporter. Strikingly, tethering of Stc1 proteins lacking one or both zinc fingers (ΔZF1, ΔZF2, and ΔZF1 +2) also generated red colonies at a similar frequency to WT, indicating that these mutants are still able to induce silencing of the *ade6*$^+$ reporter gene (Fig. 5*A*). This silencing was associated with reduced accumulation of *ade6*$^+$ transcripts and high levels of H3K9me2 on the target locus, similar to what is seen upon tethering of WT Stc1 (Fig. 5 *B* and *C*). These observations confirm that the tandem zinc finger domain is dispensable for Stc1-mediated recruitment of CLRC activity to chromatin. In fact, tethering of the Stc1 C-terminal domain alone was sufficient to trigger full silencing and heterochromatin formation, whereas no *ade6*$^+$ silencing or heterochromatin formation was observed on tethering of a Stc1 mutant protein lacking only the C-terminal domain (ΔC, Fig. 5). All the TetR-Stc1 fusion proteins were stably expressed (Fig. S7*C*). We therefore conclude that the C-terminal domain of Stc1 is necessary and sufficient to mediate association with CLRC, and hence recruitment of CLRC to chromatin.

In contrast to the tandem zinc finger domain, the C-terminal domain of Stc1 appears poorly conserved. Strikingly, however, despite a high degree of length variation, the C termini of Stc1 and its homologs in other fission yeast species are all characterized by a very high frequency of negatively charged residues, particularly aspartates (Fig. 6*A*). To investigate the functional significance of this feature, we generated Stc1 mutants in which four prominent clusters of aspartate residues (termed D-islands D1–D4, Fig. 6*A*) were replaced by alanine residues. These mutants, which were all stably expressed (Fig. S7*D*), were then tested for their ability to recruit CLRC to chromatin using the tethering assay. Mutation of the smaller D-islands D1 and D3 had only modest effects on Stc1 function (Fig. 6 *B–D*). However, mutation of D-islands D2 and D4, which contain the largest numbers of aspartates, abolished silencing mediated by tethered Stc1, as indicated by an absence of red colonies, high levels of reporter gene transcript accumulation, and complete loss of H3K9me2 from the target locus (Fig. 6 *B–D*). Thus, these aspartate-rich regions in the C terminus of Stc1 are critical to its function in recruiting CLRC to promote targeted chromatin modification.

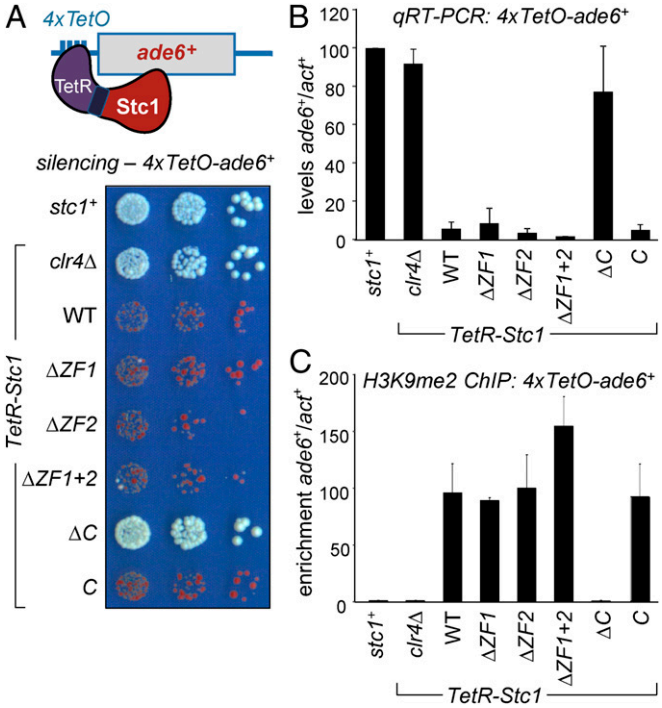

Fig. 5. Stc1 C-terminal domain is required for interaction with CLRC. (*A*) Assay for silencing at *4×TetO-ade6*$^+$ mediated by tethered Stc1 (*TetR-Stc1*). The schematic illustrates the experimental system: The reporter is an *ade6*$^+$ gene with upstream *TetO* sites (inserted at the *ura4*$^+$ locus); tethering of Stc1 is achieved by expression of a TetR-Stc1 fusion protein (integrated at *leu1*$^+$). Silencing of *ade6*$^+$ is indicated by red colonies. (*B*) Quantitative RT-PCR analysis of *ade6*$^+$ transcript levels relative to *act1*$^+$, normalized to WT ($n = 3$). (*C*) ChIP analysis of H3K9me2 levels on *4×TetO-ade6*$^+$ relative to *act1*$^+$ ($n = 3$).

Discussion

RNAi has emerged as an important mechanism for sequence-specific targeting of chromatin modifications; however, how the RNAi and chromatin modification pathways are integrated remains poorly understood in most systems. In fission yeast, association of the RNAi/RITS component Ago1 with the H3K9 methyltransferase-containing complex CLRC was recently found to be mediated by a small protein named Stc1 (31). However, little was known about the nature of the Stc1 protein or the molecular basis of these key interactions. Here, we describe the domain architecture of Stc1, which comprises a tandem zinc finger domain at the N terminus and a nonconserved, disordered C-terminal region. Functional assays indicate that the tandem zinc finger domain of Stc1 is involved in interaction with Ago1, whereas the C-terminal domain is required for interaction with CLRC.

Our detailed structural analyses indicate that the N-terminal region of Stc1 contains an unusual tandem zinc finger domain, with some similarity to LIM domains but differing in that the individual zinc fingers are largely unconstrained in their relative positioning. Mutations in ZF2 were previously found to disrupt Stc1 binding of Ago1 (31); the discovery that the two zinc fingers have the potential to function independently suggested two likely models for how Stc1 couples RNAi to chromatin modification: (*i*) ZF2 binds Ago1, and ZF1 binds CLRC, or (*ii*) the two zinc fingers function together (akin to a LIM domain) in binding Ago1, and CLRC is bound by a different domain. Several lines of evidence presented here support the latter model. First, surprisingly, deletion of ZF1 in vivo caused only a modest defect in heterochromatin formation, indicating that this domain is not essential for binding of either Ago1 or CLRC (Fig. 4 *A–E*). Second, in in vitro binding assays, although deletion of either ZF1 or ZF2

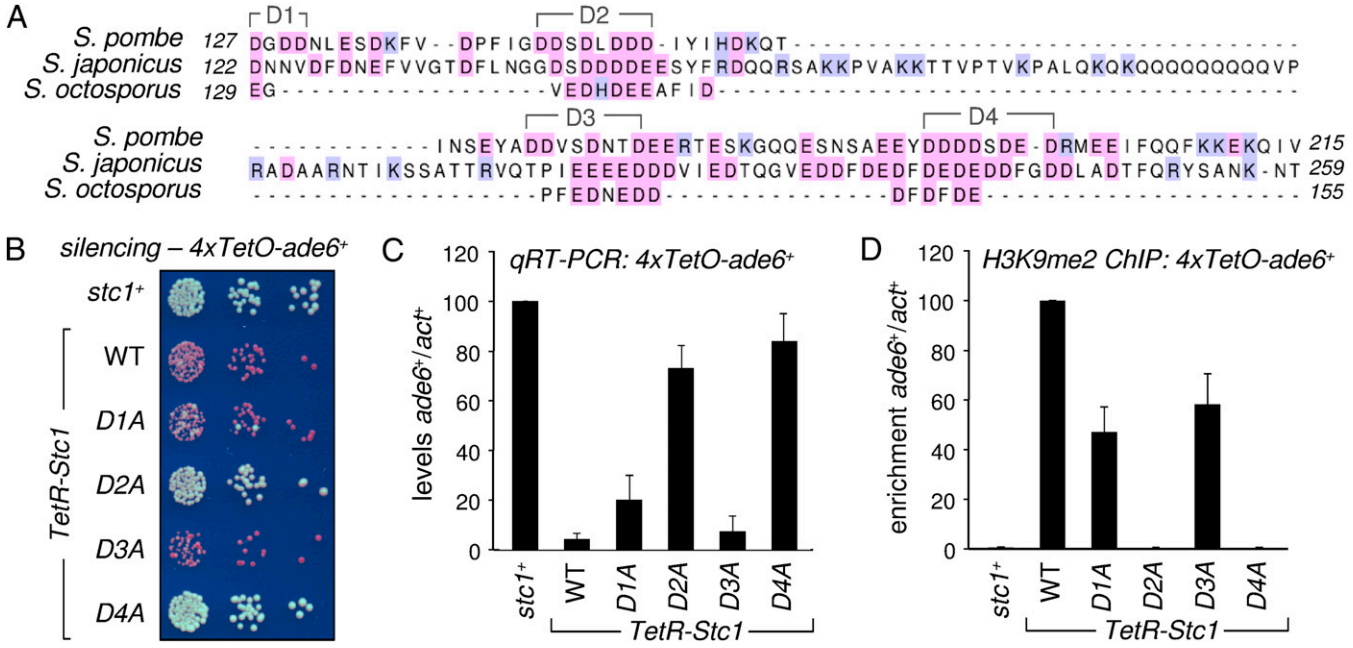

Fig. 6. Acidic residues in the Stc1 C terminus support CLRC recruitment. (*A*) Sequence alignment of the C-terminal domain of Stc1 from *S. pombe* and its close relatives *Schizosaccharomyces japonicus* (SJAG_02409.5) and *Schizosaccharomyces octosporus* (SOCG_01321.1). Negatively charged residues are shaded pink, and positively charged residues are shaded blue. D1 to D4 indicate clusters of aspartate residues mutated to alanine in *B*–*D*. (*B*) Assay for silencing at *4×TetO-ade6⁺* mediated by tethered Stc1 (*TetR-Stc1*), as in Fig. 5. (*C*) Quantitative RT-PCR analysis of *ade6⁺* transcript levels relative to *act1⁺*, normalized to WT ($n = 3$). (*D*) ChIP analysis of H3K9me2 levels on *4×TetO-ade6⁺*, relative to *act1⁺*, normalized to WT ($n = 3$).

had little effect on Ago1 binding, deletion of both ZF1 and ZF2 disrupted binding, suggesting that, in fact, both ZF1 and ZF2 have the capacity to associate with Ago1 (Fig. 4*G*). Third, pull-down and tethering assays indicated that both zinc fingers are dispensable for interaction with CLRC (Figs. 4*F* and 5). Taken together, these data suggest that both zinc fingers contribute to the recognition of Ago1, with the interaction via ZF2 being more critical in vivo; the partial loss of function caused by deletion of ZF1 in vivo most likely reflects a partial defect in Ago1 association. Possibly interaction via ZF1 helps to stabilize Stc1 association with Ago1, but a less efficient interaction in the absence of ZF1 is still sufficient to maintain moderate levels of heterochromatin. The observed flexibility between the two zinc finger motifs could also be important to facilitate recognition of Ago1 and/or contribute to its optimal embedding into the binding site.

Results from our tethering assays clearly indicate that the 90-aa C-terminal portion of Stc1 is necessary and sufficient to mediate association of CLRC (Fig. 5). Interestingly, levels of H3K9 methylation induced on tethering of Stc1 lacking the tandem zinc finger domain (ΔZF1+2) appear even higher than those induced by WT Stc1 (Fig. 5*C*). Consistent with this, we also observe slightly elevated quantities of CLRC components coprecipitating with this mutant in GST pull-down assays (Fig. 4*F*). We suspect this may reflect a conformational change in the ΔZF1+2 mutant that happens to enhance CLRC binding to the C-terminal domain. The C terminus of Stc1 is disordered in solution (Fig. 1*D* and Fig. S2). Intrinsically unstructured regions are common in eukaryotic proteins; they typically exhibit low numbers of hydrophobic residues and a high net charge, and frequently serve as binding sites for interacting proteins (39). Consistent with this, although it contains no identifiable functional motifs, the Stc1 C-terminal domain features a high frequency of negatively charged residues (39% aspartate and 21% glutamate). It is not yet known with which of the CLRC components Stc1 directly interacts. However, our observation that neutralization of acidic patches in the C-terminal domain abolishes the ability of chromatin-tethered Stc1 to trigger heterochromatin formation (Fig. 6) suggests that electrostatic interactions may play an important role in association of the Stc1 C terminus with its binding partner(s).

In higher eukaryotes, various types of small RNA can associate with different Ago proteins and effector complexes to mediate silencing in a variety of ways, at the transcriptional level (via recruitment of histone modifiers or possibly DNA methyltransferases) or posttranscriptionally (via transcript degradation or inhibition of translation initiation/elongation) (1). In many cases, an "adapter" protein like Stc1 could be expected to mediate association of a siRNA-bound Argonaute protein with a downstream effector complex. Because Argonaute proteins are highly conserved but effector partners are potentially diverse, it is the Ago interaction motif that is most likely to be conserved among such proteins. Consistent with this, although Stc1 association with CLRC is mediated by a nonconserved domain, it appears that tandem zinc finger domains (of slightly varying forms) may have conserved roles in Argonaute protein interactions. A family of mammalian LIM domain proteins was recently shown to be important for miRNA-dependent silencing, mediating association of Ago1/2 with the translation initiation factor eIF4E to bring about translational repression (32). Although the role of the LIM domain in mediating this interaction is not yet clear, it seems likely that it might have an Argonaute protein binding function, analogous to that of the tandem zinc finger domain of Stc1. Thus, LIM and LIM-like tandem zinc finger domain proteins may be good candidates for factors coupling Argonaute proteins to downstream effector complexes in a range of RNAi-related pathways throughout eukaryotes.

Materials and Methods

Cloning, Purification, and Expression. All clones were generated by PCR and sequenced to confirm identity. For structural analysis, proteins were expressed with N-terminal His_6 tags from modified PET28a(+) (GE Healthcare) vectors, in which the thrombin protease sites were substituted for tobacco etch virus (TEV) cleavage sites, in *Escherichia coli* BL21(DE3)-Gold (Stratagene) grown at 16 °C for 20 h. Proteins were purified on a Ni-chelating

column (Qiagen), treated with TEV to remove His tags, and further purified on a Ni-chelating column before size-exclusion chromatography using a Hiload 16/60 Superdex 75 column (GE Healthcare). Uniformly $^{15}N/^{13}C$- and ^{15}N-labeled proteins were prepared from cells growing in LeMaster and Richards minimal medium supplemented with 0.1 mM $ZnSO_4$, containing $^{15}NH_4Cl$ with or without $^{13}C_6$-glucose. GST-fusion proteins were expressed from PGEX-4T1 vectors in *E. coli* BL21 derivative Rosetta2(DE3)pLysS (Novagen) grown at 16 °C overnight. Proteins were purified on Glutathione Sepharose 4B (GE Healthcare).

NMR Solution Structure Determination and Refinement. All NMR spectra were acquired at 25 °C with a Bruker DMX600 spectrometer or a Varian 700-MHz spectrometer. Sample conditions for Stc1-ZF1+2$_{C38A}$ were 0.8 mM protein, 20 mM Bis-Tris·HCl (pH 6.0), and 200 mM NaCl; sample conditions for Stc1-C were 0.5 mM protein, 20 mM Bis-Tris·HCl (pH 7.0), and 150 mM NaCl. Data for chemical shift assignments for Stc1-ZF1+2 were collected using the suite of triple-resonance experiments as described previously (40). NOE distance restraints were obtained from 3D ^{15}N-resolved and ^{13}C-resolved NOESY with a mixing time of 130 ms and 110 ms, respectively. Dihedral angle restraints were obtained based on analysis of $^{13}C_\alpha$, $^{13}C_\beta$, $^{13}C'$, and ^{15}N chemical shifts using the program TALOS(+) (41, 42). Iterative manual assignment of NOEs was used to calculate the initial structures of Stc1-ZF1+2 using Xplor-NIH (version 2.28; National Institutes of Health) (43, 44). Zinc restraints were added as described previously (45). For further structure refinement, we selected hydrogen bond and RDC restraints in 3% (wt/wt) C12E5/hexanol alignment media (see below). The quality of the ensemble of 20 lowest energy structures was assessed using PROCHECK-NMR (46).

^{15}N Relaxation Measurements. Backbone amide ^1H-^{15}N NOE, ^{15}N R_1, and ^{15}N R_2 values were measured at 600 MHz with conventional pulse sequences (47). Sample conditions comprised 0.5 mM protein, 20 mM Bis-Tris·HCl (pH 7.0), and 200 mM NaCl. ^{15}N R_1 and R_2 decay was sampled at different time points [T_1 delays = 0.243, 0.011, 0.0616, 0.142, 0.243 (again), 0.364, 0.525, 0.757, and 1.15 s; T_2 delays = 0, 0.0176, 0.0352, 0.0528, 0.0704, 0.1056, 0.1408, and 0.0528 (again)]. Relaxation rates were determined by fitting peak heights as functions of relaxation decay times to a single exponential decay function using SPARKY 3 (provided by T. D. Goddard and D. G. Kneller, University of California, San Francisco). Mean R_2/R_1 ratios were calculated after excluding residues with ^1H-^{15}N NOE < 0.6. The ^1H-^{15}N NOE values were calculated from the ratios of peak intensities with and without proton saturation. Errors in peak intensities were estimated from the average baseline noise.

RDCs. RDCs were determined in two alignment media. The liquid crystalline medium was prepared from a mixture of pentaethylene glycol monododecyl ether (C12E5; Sigma) and 6-hexanol (0.87 molar ratio) (48). C12E5 was used at a final concentration of 3% (wt/wt) in a 90% H_2O/10% D_2O solution. Polyacrylamide gels were prepared as described previously and squeezed into an open-ended NMR tube (49). Sample alignment was monitored via splitting of the deuterium signal. N-H heteronuclear dipolar couplings were measured at 600 MHz using the in-phase and anti-phase (IPAP) scheme (50). RDC values were obtained by subtracting the reference value of the protein in isotropic solution. Two duplicate datasets were collected for each RDC experiment. For data analysis, we used PALES (51); dipolar couplings from residues having lower ^1H-^{15}N NOEs (<0.6; residues 36, 65–68, and 124–126) were excluded. The Q value was used to assess the agreement between experimental and theoretical values. The final 20 lowest energy structures were used as models.

CD Spectroscopy. Far-UV CD spectra were recorded at 25 °C with a Jasco-810 spectropolarimeter, at wavelengths between 190 and 260 nm, using a 0.1-cm path length cell and 100-μg/mL protein sample in 50 mM PBS (pH 7.0). A buffer-only reference was subtracted from each curve.

Yeast Strains and Plasmids. *S. pombe* strains are listed in Table S2. Standard procedures were used for growth and genetic manipulations (52). For genomic insertion of Stc1 mutants, corresponding PCR fragments were integrated via homologous recombination by replacement of *stc1:ura4*$^+$. The TetR-Stc1 tethering system was described previously (31). For tethering of Stc1 mutants, corresponding PCR products were cloned into pDUAL-TetR-2× FLAG, and Not1-digested plasmid was integrated at *leu1*$^+$.

GST Pull-Down and in Vitro Binding Assays. GST pull-downs were performed using cell lysates from *S. pombe* strains expressing multiple epitope-tagged CLRC components (Rik1-myc/flag-Clr4 or Dos2-flag/gfp-Dos1). *S. pombe* cells were grown to a density of 1×10^8 cells/mL in 4× yeast extract with supplements (YES) medium, lysed mechanically, and resuspended in cold lysis buffer [50 mM Hepes (pH 7.5), 150 mM NaCl, 5 mM EDTA, 0.1% Nonidet P-40, 5 mM DTT, 1 mM PMSF, and protease inhibitors]. Following centrifugation and preclearing, the prepared lysate was divided into six equal fractions and each fraction was incubated with Glutathione Sepharose 4B beads plus ∼100 μg of GST-fusion protein (or an equimolar concentration of GST alone as a control) for 3 h at 4 °C. Samples were washed four times in lysis buffer and analyzed by SDS/PAGE. Antibodies used for Western blotting were anti-flag M2 (Sigma), anti-c-myc (Roche), and anti-GFP (Roche), all at a 1:1,000 dilution, and anti-GST at a 1:2,500 dilution.

For in vitro binding assays, ^{35}S-labeled Ago1 protein was produced with a TNT T7 kit (Promega) and incubated with 4 μg of GST fusion protein in binding buffer (1× PBS, 0.5 mM DTT, 1 mM PMSF, 0.5 mg/mL BSA, and protease inhibitors) for 30 min on ice. Glutathione Sepharose 4B was added and incubated for 1 h, followed by four washes in binding buffer. Samples were analyzed by SDS/PAGE and fluorography.

Chromatin and RNA Analysis. H3K9me2 ChIP was performed as described previously (53), using monoclonal H3K9me2 antibody (m5.1.1) (54). Relative enrichments were calculated as the ratio of the product of interest to the control product (*act1*$^+$) in immunoprecipitate over input. Northern blot analysis of centromeric siRNAs and quantitative RT-PCR analysis of transcripts were performed as described previously (28). Quantitative PCR primers and primers used as siRNA probes are listed in Table S3. In all cases, histograms represent three biological replicates and error bars represent 1 SD.

ACKNOWLEDGMENTS. We thank J. Jin for helpful suggestions and T. Owen-Hughes for critical reading of the manuscript. We are grateful to T. Urano for provision of anti-H3K9me2 antibody and the Division of Signal Transduction Therapy (University of Dundee) for anti-GST antibody and also thank F. Delaglio and A. Bax for providing the software NMRPipe; T. D. Goddard and D. G. Kneller for providing Sparky; G. M. Clore, J. Kuszewski, C. D. Schwieters, and N. Tjandra for providing Xplor-NIH; and W. L. DeLano for providing pyMol. This work was financially supported by the National Basic Research Program of China (973 Program Grants 2011CB966302, 2012CB917201, and 2011CB911104); the Chinese National Natural Science Foundation (Grants 30830031 and 31170693); the Priority Research Program of the Chinese Academy of Sciences; the European Union Seventh Framework Programme Network of Excellence "EpiGeneSys" (Grant 257082); and UK Medical Research Council Career Development Award G1000505/1 (to E.H.B.).

1. Ghildiyal M, Zamore PD (2009) Small silencing RNAs: An expanding universe. *Nat Rev Genet* 10(2):94–108.
2. Lejeune E, Allshire RC (2011) Common ground: Small RNA programming and chromatin modifications. *Curr Opin Cell Biol* 23(3):258–265.
3. Verdel A, Vavasseur A, Le Gorrec M, Touat-Todeschini L (2009) Common themes in siRNA-mediated epigenetic silencing pathways. *Int J Dev Biol* 53(2-3):245–257.
4. Bannister AJ, et al. (2001) Selective recognition of methylated lysine 9 on histone H3 by the HP1 chromo domain. *Nature* 410(6824):120–124.
5. Zhang K, Mosch K, Fischle W, Grewal SI (2008) Roles of the Clr4 methyltransferase complex in nucleation, spreading and maintenance of heterochromatin. *Nat Struct Mol Biol* 15(4):381–388.
6. Sadaie M, Iida T, Urano T, Nakayama J (2004) A chromodomain protein, Chp1, is required for the establishment of heterochromatin in fission yeast. *EMBO J* 23(19):3825–3835.
7. Grewal SI, Bonaduce MJ, Klar AJ (1998) Histone deacetylase homologs regulate epigenetic inheritance of transcriptional silencing and chromosome segregation in fission yeast. *Genetics* 150(2):563–576.
8. Nakayama J, Rice JC, Strahl BD, Allis CD, Grewal SI (2001) Role of histone H3 lysine 9 methylation in epigenetic control of heterochromatin assembly. *Science* 292(5514):110–113.
9. Shankaranarayana GD, Motamedi MR, Moazed D, Grewal SI (2003) Sir2 regulates histone H3 lysine 9 methylation and heterochromatin assembly in fission yeast. *Curr Biol* 13(14):1240–1246.
10. Li F, et al. (2005) Two novel proteins, dos1 and dos2, interact with rik1 to regulate heterochromatic RNA interference and histone modification. *Curr Biol* 15(16):1448–1457.
11. Horn PJ, Bastie JN, Peterson CL (2005) A Rik1-associated, cullin-dependent E3 ubiquitin ligase is essential for heterochromatin formation. *Genes Dev* 19(14):1705–1714.
12. Thon G, et al. (2005) The Clr7 and Clr8 directionality factors and the Pcu4 cullin mediate heterochromatin formation in the fission yeast Schizosaccharomyces pombe. *Genetics* 171(4):1583–1595.
13. Jia S, Kobayashi R, Grewal SI (2005) Ubiquitin ligase component Cul4 associates with Clr4 histone methyltransferase to assemble heterochromatin. *Nat Cell Biol* 7(10):1007–1013.

14. Hong EJ, Villén J, Gerace EL, Gygi SP, Moazed D (2005) A cullin E3 ubiquitin ligase complex associates with Rik1 and the Clr4 histone H3-K9 methyltransferase and is required for RNAi-mediated heterochromatin formation. *RNA Biol* 2(3):106–111.
15. Buscaino A, et al. (2012) Raf1 Is a DCAF for the Rik1 DDB1-like protein and has separable roles in siRNA generation and chromatin modification. *PLoS Genet* 8(2): e1002499.
16. Jia S, Noma K, Grewal SI (2004) RNAi-independent heterochromatin nucleation by the stress-activated ATF/CREB family proteins. *Science* 304(5679):1971–1976.
17. Kanoh J, Sadaie M, Urano T, Ishikawa F (2005) Telomere binding protein Taz1 establishes Swi6 heterochromatin independently of RNAi at telomeres. *Curr Biol* 15(20):1808–1819.
18. Hansen KR, Ibarra PT, Thon G (2006) Evolutionary-conserved telomere-linked helicase genes of fission yeast are repressed by silencing factors, RNAi components and the telomere-binding protein Taz1. *Nucleic Acids Res* 34(1):78–88.
19. Kim HS, Choi ES, Shin JA, Jang YK, Park SD (2004) Regulation of Swi6/HP1-dependent heterochromatin assembly by cooperation of components of the mitogen-activated protein kinase pathway and a histone deacetylase Clr6. *J Biol Chem* 279(41):42850–42859.
20. Volpe TA, et al. (2002) Regulation of heterochromatic silencing and histone H3 lysine-9 methylation by RNAi. *Science* 297(5588):1833–1837.
21. Bühler M, Moazed D (2007) Transcription and RNAi in heterochromatic gene silencing. *Nat Struct Mol Biol* 14(11):1041–1048.
22. Grewal SIS (2010) RNAi-dependent formation of heterochromatin and its diverse functions. *Curr Opin Genet Dev* 20(2):134–141.
23. Lejeune E, Bayne EH, Allshire RC (2010) On the connection between RNAi and heterochromatin at centromeres. *Cold Spring Harb Symp Quant Biol* 75:275–283.
24. Kloc A, Zaratiegui M, Nora E, Martienssen R (2008) RNA interference guides histone modification during the S phase of chromosomal replication. *Curr Biol* 18(7):490–495.
25. Chen ES, et al. (2008) Cell cycle control of centromeric repeat transcription and heterochromatin assembly. *Nature* 451(7179):734–737.
26. Motamedi MR, et al. (2004) Two RNAi complexes, RITS and RDRC, physically interact and localize to noncoding centromeric RNAs. *Cell* 119(6):789–802.
27. Sugiyama T, Cam H, Verdel A, Moazed D, Grewal SIS (2005) RNA-dependent RNA polymerase is an essential component of a self-enforcing loop coupling heterochromatin assembly to siRNA production. *Proc Natl Acad Sci USA* 102(1):152–157.
28. Bayne EH, et al. (2008) Splicing factors facilitate RNAi-directed silencing in fission yeast. *Science* 322(5901):602–606.
29. Schalch T, et al. (2009) High-affinity binding of Chp1 chromodomain to K9 methylated histone H3 is required to establish centromeric heterochromatin. *Mol Cell* 34(1):36–46.
30. Creamer KM, Partridge JF (2011) RITS-connecting transcription, RNA interference, and heterochromatin assembly in fission yeast. *Wiley Interdiscip Rev RNA* 2(5):632–646.
31. Bayne EH, et al. (2010) Stc1: A critical link between RNAi and chromatin modification required for heterochromatin integrity. *Cell* 140(5):666–677.
32. James V, et al. (2010) LIM-domain proteins, LIMD1, Ajuba, and WTIP are required for microRNA-mediated gene silencing. *Proc Natl Acad Sci USA* 107(28):12499–12504.
33. Blake PR, Park JB, Adams MWW, Summers MF (1992) Novel observation of Nh...S(Cys) hydrogen-bond-mediated scalar coupling in Cd-113-substituted rubredoxin from Pyrococcus-furiosus. *J Am Chem Soc* 114(12):4931–4933.
34. Babini E, Bertini I, Capozzi F, Chirivino E, Luchinat C (2006) A structural and dynamic characterization of the EF-hand protein CLSP. *Structure* 14(6):1029–1038.
35. Losonczi JA, Andrec M, Fischer MWF, Prestegard JH (1999) Order matrix analysis of residual dipolar couplings using singular value decomposition. *J Magn Reson* 138(2): 334–342.
36. Holm L, Sander C (1995) Dali: A network tool for protein structure comparison. *Trends Biochem Sci* 20(11):478–480.
37. Krishna SS, Majumdar I, Grishin NV (2003) Structural classification of zinc fingers: Survey and summary. *Nucleic Acids Res* 31(2):532–550.
38. Grishin NV (2001) Treble clef finger—A functionally diverse zinc-binding structural motif. *Nucleic Acids Res* 29(8):1703–1714.
39. Schlessinger A, Punta M, Rost B (2007) Natively unstructured regions in proteins identified from contact predictions. *Bioinformatics* 23(18):2376–2384.
40. Clore GM, Gronenborn AM (1994) Multidimensional heteronuclear nuclear magnetic resonance of proteins. *Methods Enzymol* 239:349–363.
41. Cornilescu G, Delaglio F, Bax A (1999) Protein backbone angle restraints from searching a database for chemical shift and sequence homology. *J Biomol NMR* 13(3): 289–302.
42. Shen Y, Delaglio F, Cornilescu G, Bax A (2009) TALOS+: A hybrid method for predicting protein backbone torsion angles from NMR chemical shifts. *J Biomol NMR* 44(4):213–223.
43. Schwieters CD, Kuszewski JJ, Tjandra N, Clore GM (2003) The Xplor-NIH NMR molecular structure determination package. *J Magn Reson* 160(1):65–73.
44. Schwieters CD, Kuszewski JJ, Clore GM (2006) Using Xplor-NIH for NMR molecular structure determination. *Prog Nucl Magn Reson Spectrosc* 48(1):47–62.
45. Simonson T, Calimet N (2002) Cys(x)His(y)-Zn2+ interactions: Thiol vs. thiolate coordination. *Proteins* 49(1):37–48.
46. Laskowski RA, Rullmannn JA, MacArthur MW, Kaptein R, Thornton JM (1996) AQUA and PROCHECK-NMR: Programs for checking the quality of protein structures solved by NMR. *J Biomol NMR* 8(4):477–486.
47. Kay LE, Torchia DA, Bax A (1989) Backbone dynamics of proteins as studied by 15N inverse detected heteronuclear NMR spectroscopy: Application to staphylococcal nuclease. *Biochemistry* 28(23):8972–8979.
48. Otting G, Ruckert M (2000) Alignment of biological macromolecules in novel nonionic liquid crystalline media for NMR experiments. *J Am Chem Soc* 122(32):7793–7797.
49. Chou JJ, Gaemers S, Howder B, Louis JM, Bax A (2001) A simple apparatus for generating stretched polyacrylamide gels, yielding uniform alignment of proteins and detergent micelles. *J Biomol NMR* 21(4):377–382.
50. Ottiger M, Delaglio F, Bax A (1998) Measurement of J and dipolar couplings from simplified two-dimensional NMR spectra. *J Magn Reson* 131(2):373–378.
51. Zweckstetter M (2008) NMR: prediction of molecular alignment from structure using the PALES software. *Nat Protoc* 3(4):679–690.
52. Moreno S, Klar A, Nurse P (1991) Molecular genetic analysis of fission yeast Schizosaccharomyces pombe. *Methods Enzymol* 194:795–823.
53. Pidoux A, Mellone B, Allshire R (2004) Analysis of chromatin in fission yeast. *Methods* 33(3):252–259.
54. Nakagawachi T, et al. (2003) Silencing effect of CpG island hypermethylation and histone modifications on O6-methylguanine-DNA methyltransferase (MGMT) gene expression in human cancer. *Oncogene* 22(55):8835–8844.